



A multispectral resonant waveguide nanopatterned chip for robust oil quality monitoring



K. Bougot-Robin^{a,1,2}, W. Cao^{b,1}, S. Li^{b,3}, H. Benisty^c, W. Wen^{b,*}

^a Institute for Advanced Study, Hong Kong University of Science and Technology, Hong Kong

^b Physics Department, Hong Kong University of Science and Technology, Hong Kong

^c Laboratoire Charles Fabry, Institut Optique Graduate School, CNRS, Université Paris Sud, France

ARTICLE INFO

Article history:

Received 2 December 2014

Received in revised form 29 March 2015

Accepted 31 March 2015

Available online 15 April 2015

Keywords:

Microarray imaging

Resonant waveguide

Biosensing

Oil refractive index

Multispectral

Microfluidic integration

ABSTRACT

Oil quality control is an important issue in the food industry and consumer market. Consequently, on-site control with a user-friendly device at a reasonable cost is needed. Simple optical imaging of resonant peak on a nanostructured chip by a consumer grade camera allows real-time label-free biomolecules sensing and bulk refractive index measurements. Multispectral capability on the same nanostructured chip is introduced for the first time here, both through theory and experiments. We demonstrate that with optimized nanostructuring, the whole visible spectrum can be sensed using the same chip support. By analyzing oil samples from deep frying process, we found cooking process can induce a small ($\sim 10^{-3}$) but stable and detectable change of the refractive due to the accumulation of polar materials. This is measured accurately thanks to the high-sensitivity of our refractive index sensing chip ($\Delta n \sim \pm 1 \times 10^{-5}$). Refractive index change of a mixture of animal fat and vegetable oil is also studied. We compare refractive index change at the 2 extremities of the visible spectrum ($\lambda = 480$ nm and $\lambda = 630$ nm), and confirm and ~ 2 times larger change for small wavelength. Possible integration of our device with powerful imaging capability in recent popular smartphones is also discussed.

© 2015 Elsevier B.V. All rights reserved.

1. Introduction

1.1. Oil refractive index sensing

In food production or safety inspection areas it is foremost important to dispose of reliable and convenient devices for on-site oil quality monitoring of edible oils [1]. Indeed, a long and repeated heating of oil induces a series of degradation reactions, such as oxidation, polymerization and hydrolysis. This results in organoleptic deterioration and a decrease in nutrition value. Many of the degradation products are harmful to health as they cause vitamin destruction, enzyme inhibition, and gastrointestinal irritations and might also cause mutations [2].

For its severity of influence and difficulty of accurate identification, china government even requested public proposals to identify

the “gutter oil”—a slang word for resold cooking oil refined from used oil [3].

One common criterion for oil quality is its color. Other determination criteria like total polar material determination, acid value or iodine value, are well established characterizations but they are usually performed in a laboratory environment and are time consuming. Considering the need of on-site analysis and fast response, it is of foremost importance to dispose of reliable and convenient devices for oil quality testing purpose.

We propose here a measurement platform based on high sensitivity refractive index measurement performed by simple imaging of a chip patterned with nanogratings. The nanostructuring is designed such that sensing can be carried out at several wavelengths, but using the same chip support.

Color measurement is a simple indicator of oil quality [4]. It is used in pre or post industrialization for instance with colorimeters such as Lovibond [5]. Nevertheless, it has limited accuracy and might be subject to personal bias. Thus some objective and quantitative criteria are desirable. Additionally, color may be falsified by oil mixtures.

By doing refractive index and absorption sensing of oils, different oils might be differentiated and their quality might be controlled as well. The possibility to discard mixtures mimicking

* Corresponding author. Tel.: +852 2358 7979; fax: +852 2358 1652.

E-mail addresses: kristelle.robins@yahoo.fr (K. Bougot-Robin), wcaao@ust.hk (W. Cao), phwen@ust.hk (W. Wen).

¹ These authors contribute equally to this work.

² Current address: Chemistry Department, Imperial College, London, United Kingdom.

³ Current address: School of Chemistry, University of Leeds, United Kingdom.

a good oil based on color is one of the interesting perspectives of this work.

1.2. “Peak-tracking chip” technique

The “Peak-tracking chip” technique is a label-free direct imaging technique, which successfully combines the advantages of resonant waveguide grating (RWG) label-free detection and of direct imaging with minimized demand [6]. RWG have some advantages in term of optimized light-matter interaction with immobilized biomolecules or analyte [7]. Such an optimization can be achieved through detection wavelengths, material refractive indices and geometrical parameters of the chip [8]. RWGs based sensing is realized by measuring the shift of the resonance profile, usually of Fano lineshapes [9]. While this is usually achieved by varying an instrumental parameter (wavelength or angle) [10,11], we recently demonstrated that the intensity profile might be integrated in the chip itself in order to become a spatial image. This allows robust and sensitive sensing with consumer-grade CMOS camera [6,12]. This is a significant advantage in term of cost and simplicity, which are highly desired for biosensing or on-site oil testing. Exploiting bi-dimensionality of the resonant chip nanostructuration, multi-spectral sensing can also be implemented on the same chip support. This is a significant advantage in comparison to usual RWGs sensing techniques [8,10,11], involving a single grating and therefore a single resonant wavelength domain.

Spatial Fano profiles in direct imaging are achieved by slowly varying a geometrical parameter of the grating on a resonant waveguide chip. The work presented first emphasizes monochromatic imaging and sensing. The chip and detection set-up are illustrated in Fig. 1(A) for monochromatic sensing. Multiple sensing tracks can be placed on the same chip, as illustrated in Fig. 1(B) to perform 2D array sensing [6,13]. Each sensing area consists of a track of M nanogratings micropads, these latter having a smoothly varying geometry (and therefore resonant condition) as schemed in Fig. 1(C). The chip presented here corresponds to monochromatic sensing, with identical tracks (same nanostructuration) placed in an array format.

The technique has 2 types of applications: label-free bioarray imaging and bulk solution refractive index sensing. The nanostructuration is chosen depending on the targeted detection wavelength and index range. Real-time DNA hybridization with high sensitivity

has recently been demonstrated through the detection of single nucleotide polymorphism. Details on the biology process and fluidic integration of our technique may be found in [14]. Bulk sensing has been demonstrated with known calibrated solutions at a single wavelength $\lambda = 545$ nm, demonstrating a refractive index span of [1.33–1.48] on a single track with filling factor $f_i = [0.3–0.7]$, and a wavelength $\lambda = 545$ nm [6].

We demonstrate here the potential of our technique for oil refractive index sensing, and more specifically taking benefit of sensitivity and multispectral potential. Our chip-based detection technique is also advantageous in term of device simplicity, low amount of analyte required and fast response.

2. Multispectral sensing

2.1. Spectrally selective tracks

Our technique is able to measure refractive index variation down to $\Delta n \sim \pm 1 \times 10^{-5}$, as demonstrated through theory and experiments [13]. Sensitive near resonance detection are usually limited to only one wavelength (as the chip has only one resonant condition) [10,11]. Here, by exploiting the nanopattern parameters, we demonstrate that different wavelengths may be sensed using the same chip. More specifically, we make tracks of grating micropads of different periods, thus targeting a different wavelength domain on a given column. Discrete profile values allowing the essential resonance scan are obtained by slowly varying the groove width (and consequently the filling factor) in the vertical direction along a track.

2.2. Multispectral chip design

Electromagnetic properties are calculated using scattering matrix formalism [15,16].

Specifically, to demonstrate that the whole visible spectrum can be sensed using the same chip support, we design tracks with periods $\Lambda_b = 380$ nm for sensing at $\lambda_b \sim 480$ nm, $\Lambda_g = 440$ nm for sensing at $\lambda_g \sim 545$ nm and $\Lambda_r = 520$ nm for sensing at $\lambda_r \sim 630$ nm. Thickness of the layers and etching depth are the same for all tracks, allowing a simpler fabrication process through electron beam lithography patterning. A chip with a set of tracks of different periods is presented in Fig. 2 with (A) side-view and (B) top-view.

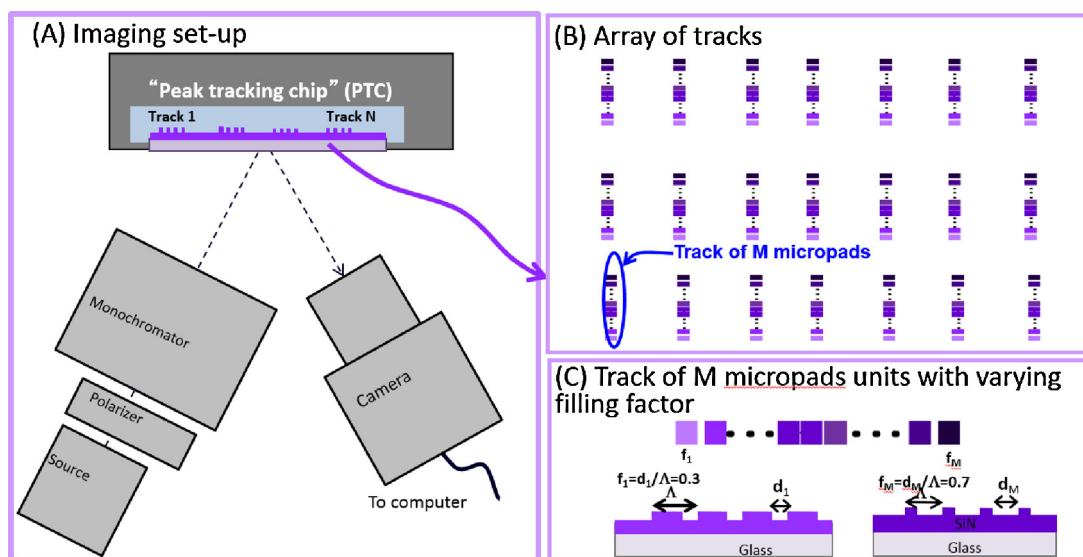


Fig. 1. Technique overview (A) imaging set-up of 2D array nanopatterned chip, (B) array of tracks, (C) track nanostructuration with single period Λ and varying groove with d_i .

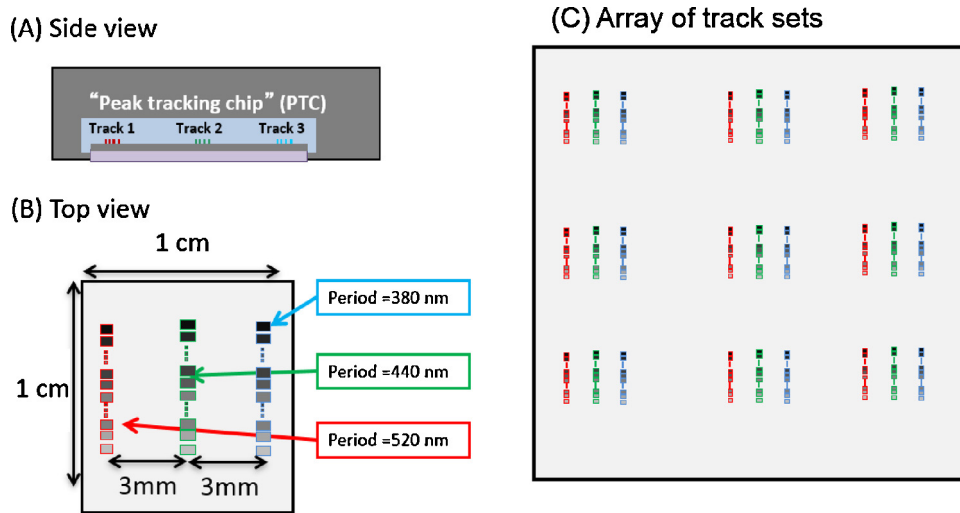


Fig. 2. Technique overview (A) imaging set-up of 2D array nanopatterned chip of different tracks on its surface, (B) chip with 3 different tracks targeting different resonant wavelengths, (C) multiplex chip scheme with several sets of tracks, targeting different wavelengths.

In Fig. 2(C), we give a scheme of a multiplex chip with sets of tracks placed in a 2D geometry. By adjusting tracks dimensions and distance between tracks, a few dozens of biological sensing area or bulk refractive index sensing can be implemented on a few cm² chip. To introduce a sample on a given ‘track set’, independent fluidic chambers separated by O-rings might be implemented [14].

The resonant response of each track (being itself composed by an ensemble of micropads of different filling factors) is calculated at its specific resonant response versus excitation wavelength. In this work, we study oil sensing. Photonic properties are therefore calculated for bulk solutions with index in the range [1.4–1.5]. The filling factor is varied in the range $f \sim [0.3–0.7]$. This is achieved by a change of the groove width by step of 4 nm (smallest variation achievable with our electron beam lithography equipment and associated software). In Table 1, we report the geometrical parameters for various periods, namely $\Lambda_b \equiv 380$ nm, $\Lambda_g \equiv 440$ nm, and $\Lambda_r \equiv 520$ nm used for sensing at their corresponding resonant wavelengths. The groove widths in nm as well as the thickness of the layers are also reported in period unit. An excitation angle $\theta \sim 20^\circ$, allows near normal imaging with the whole chip “in focus”.

In Fig. 3, we give the simulated reflectivity maps depending of the filling factor ($\sim [0.3–0.7]$) and the refractive index of the bulk solution ($\sim [1.4–1.5]$). Fig. 3(A–C) correspond to sensing at wavelength $\lambda_b = 480$ nm, $\lambda_g = 545$ nm and $\lambda_r = 630$ nm for tracks periods of $\Lambda_b \equiv 380$ nm, $\Lambda_g = 440$ nm and $\Lambda_r = 520$ nm respectively.

For a better insight of analyzed images, we give in Fig. 3(D–F) simulated images of tracks at each of the wavelength. Each of the section consists in a selection of 15 micropads around the spatial resonance peak, for an analyte refractive index $n = 1.45$.

In “period unit” Δ , the layers thicknesses, etching depth, groove width step are larger for the smallest periods. This affects photonic properties, as revealed through diffraction efficiency and resonance quality factor. We obtain higher maximal diffraction efficiency for smaller wavelengths, as well as narrower profiles on a given filling factor range Δf .

For each configuration, we determined the refractive index change per micropad, which can be termed a sensitivity. Values are noted as PMS, stating for ‘per-micropad-sensitivity’. For all cases, we report in Table 2 the change of resonance position induced by a change of refractive index $\Delta n = 0.1$, as well as PMS values. From the diffraction efficiency maps, we see that for $\Lambda_b \equiv 380$ nm with $\lambda_b = 480$ nm, a change of refractive index $\Delta n = 0.1$ induces a shift of 20 micropads or $\Delta f = 0.154$. It corresponds to a sensitivity $\text{PMS} = 5 \times 10^{-3}$ RIU/micropad unit. As we

will see in what follows, studied samples have a refractive index $n \sim 1.47 \pm 5 \times 10^{-3}$. Considering the local slope, the change in sensitivity is slightly decreased to $\text{PMS}_b = 4.2 \times 10^{-3}$ RIU/micropad. At $\Lambda_g \equiv 480$ nm with $\lambda_g = 545$ nm, a change $\Delta n = 0.1$ induces a change of ~ 30 micropad unit or $\Delta f = 0.273$. It corresponds to a change in sensitivity $\text{PMS} = 3.3 \times 10^{-3}$ RIU/micropad unit, decreasing to $\text{PMS}_g = 3.1 \times 10^{-3}$ RIU/micropad unit when using the local slope at $n = 1.47$. Concerning imaging in red, with the conditions of $\Lambda_r \equiv 520$ nm with $\lambda_r = 630$ nm, a change in refractive index $\Delta n = 0.1$ induces a change of ~ 46 micropad unit or $\Delta f = 0.4842$. It corresponds to a global sensitivity $\text{PMS} = 2.2 \times 10^{-3}$ RIU/micropad unit, decreasing to $\text{PMS}_r = 1.9 \times 10^{-3}$ RIU/micropad unit when using the local slope at $n = 1.47$. The ratio of the sensitivities per micropad in refractive index between extreme wavelength $\lambda_b = 480$ nm and $\lambda_r = 630$ nm is of $\text{PMS}_b/\text{PMS}_r = 2.2$.

In the visible range, as done here (less than an octave in lambda) the change in sensitivity is the main factor. The change of detection accuracy depends on many factors, such as pad size, and could be optimized, but its variations are a second order issue in our wavelength range.

3. Experimental

3.1. Experimental set-up

The set-up is a reflective direct imaging set-up as illustrated in Fig. 1(A). A high power white LED (Thorlab Inc.) is focused on the entrance slit of a monochromator. The wavelength is chosen to perform sensing at the resonant wavelength of a given track. The spectral width is adjusted to $\Delta\lambda = 0.1$ nm. The light is collimated to illuminate the nanopatterned chip, and has an angular width $\Delta\theta = 0.1^\circ$. A polarizer selects a TM polarization which is more dispersive and therefore allows a better sensitivity. Raw images of the chip are recorded by a Canon EOS 5D camera with 16 bit depth for optimal digitization of 1.5×10^{-5} precision. The CMOS sensor of our digital camera (Canon 5D Mark II) have sensor size of 5616×3744 pixels, with a pixel pitch of 6.4 micron. The read-out noise is 2.5 electrons, with a full well of 65,700 e, and till $10\times$ better than commercially available CCD sensors [12]. Note that this digital camera sensor is over-performing for our application would still be suitable. We also demonstrated good robustness to noise from our peak position determination [13]. With these instrumental parameters, the integration time is 1 s. Measured images are averaged over 5 images before analysis, giving a ~ 10 s acquisition

Table 1
Chip geometrical parameters.

Period (nm)	Grating depth (period unit)	SiN layer thickness	$\Delta f_{\text{step}} = 4 \text{ nm}/\Lambda$	Groove width range (nm)	Number of tracks to cover $\Delta f \sim [0.3\text{--}0.7]$
$\Lambda_b = 380 \text{ nm}$	0.174	0.313	0.00769	116–264	37
$\Lambda_g = 440 \text{ nm}$	0.150	0.270	0.00909	136–304	43
$\Lambda_r = 520 \text{ nm}$	0.127	0.228	0.01053	160–360	51

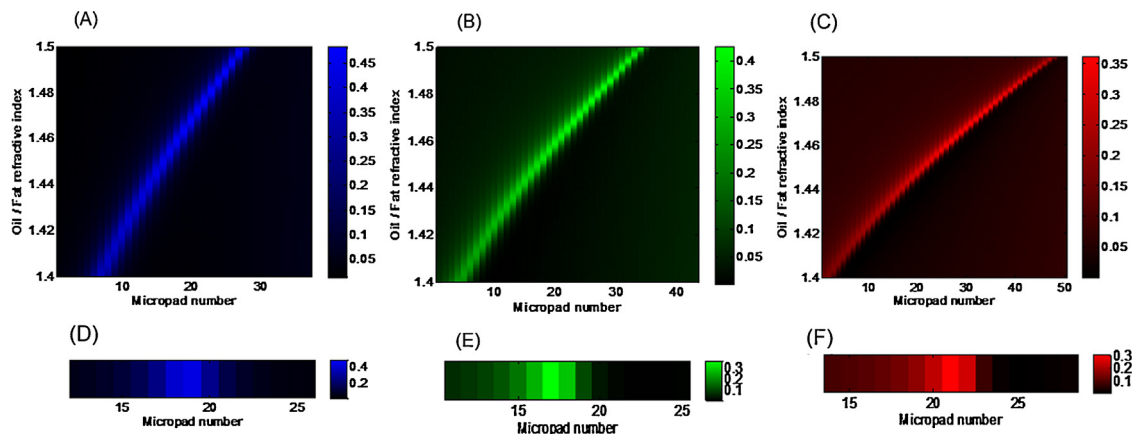


Fig. 3. Diffraction efficiency maps for a range of filling factor $\sim [0.3\text{--}0.7]$ and a range of bulk index $[1.4\text{--}1.5]$ (A) for track of period $\Lambda_b = 380 \text{ nm}$ and monochromatic imaging at $\lambda = 480 \text{ nm}$, (B) for track of period $\Lambda_g = 440 \text{ nm}$ and monochromatic imaging at $\lambda = 545 \text{ nm}$ and (C) for track of period $\Lambda_r = 520 \text{ nm}$ and monochromatic imaging at $\lambda = 630 \text{ nm}$ (D–F) images corresponding to a bulk index $n \sim 1.45$, on a 15 micropads selection corresponding to the (A–C) cases respectively.

time. This is adequate for most sensing applications, including real-time sensitive biological sensing [14]. Micropads have dimensions of $90 \times 200 \mu\text{m}$, with $10 \mu\text{m}$ interspacing in the vertical direction. The distance between tracks is 3 mm. The three tracks are nearly seen in focus thanks to the small incidence angle $\theta \sim 20^\circ$.

3.2. Nanopattern design and chip fabrication

The chip consists in a soda lime glass substrate covered by a thin silicon nitride layer, for guiding purpose. We neglect dispersion of materials over the visible range and use refractive indices obtained at $\lambda = 545 \text{ nm}$. For the substrate, we use $n = 1.471$ from the provider data, and for SiN, we use ellipsometry characterization and obtain an index ($n \sim 2.1 + 0.002i$). Modal dispersion stemming from the thin nitride thickness is much larger than chromatic dispersion.

The nanostructure of the SiN layer is chosen to guide light around a wavelength of interest and perform subsequent sensing. The chip design has been described before, and each track has a period $\Lambda_b = 380 \text{ nm}$, $\Lambda_g = 440 \text{ nm}$ and $\Lambda_r = 520 \text{ nm}$, with filling factor in the range $[0.3\text{--}0.7]$ obtained by groove width variation. The nanopattern is fabricated using electron beam lithography process using a JEOL JBX-6300FS equipment. The fabrication process has been detailed in [6]. As a result of electron beam lithography equipment performances, the minimal groove width variation is $\Delta g = 4 \text{ nm}$, corresponding to a variation of the filling factor $\Delta f_{380\text{nm}} = 10.5 \times 10^{-3}$, $\Delta f_{440\text{nm}} = 8.9 \times 10^{-3}$ and $\Delta f_{520\text{nm}} = 6.4 \times 10^{-3}$ respectively. Therefore a higher profile digitization is obtained for larger wavelength. Experimental images of such tracks illuminated at their resonant wavelength under the

same incident angle of $\theta \sim 20^\circ$ are given in Fig. 4. The illumination wavelengths are chosen to excite the tracks under their resonant condition, as witnessed by the varying intensity over the tracks, with a Fano lineshape profile [8]. This confirms that with different incident wavelengths, the whole visible spectrum might be assessed on a single chip support. Sensing with higher number of spectral values on the same chip (1 track for periods ranging from $\Lambda = 330$ to $\Lambda = 570 \text{ nm}$ by step of 10 nm for sensitive sensing on the whole visible spectrum) is also under study. An optical set-up allowing illumination of each track at its resonant wavelength at a time is an interesting possibility for multispectral sensing. This would allow sensitive sensing of small sample volume on the whole visible spectrum at a time. This can be implemented using dispersion compensation [17], for instance, prism pair [18] or grating pairs [19], thus allowing vertical multiplexing of set of tracks. Further beam splitting might be implemented for horizontal multiplexing.

3.3. Sample preparation

Two types of samples are tested in this work: deep-fried sunflower oil samples with a different number of cooking cycles and animal fat/sunflower oil mixtures.

Concerning oil refractive index changes through the cooking process, we use potato chips as the food sample and deep-fry them in sunflower oil at $180\text{--}185^\circ\text{C}$. The initial oil volume is 1.8 L, and at each cycle 60 g fresh frozen potato chips are immersed in heated oil for 5 min and then taken out. We then wait for 25 min without any food in the oil, before starting a new cycle. The frying process is interrupted every 5 cycles, where we wait for the oil to cool

Table 2
Track sensitivities.

Period (nm)	λ (nm)	Δf induced by $\Delta n = 0.1$ in the fluid	Global sensitivity (average PMS in RIU/micropad)	Local sensitivity (PMS in RIU/micropad)	$\Delta n/\Delta f$
$\Lambda_b = 380$	480	0.15385	5×10^{-3}	4.2×10^{-3}	0.546
$\Lambda_g = 440$	520	0.27273	3.3×10^{-3}	3.1×10^{-3}	0.341
$\Lambda_r = 520$	630	0.48421	2.2×10^{-3}	1.9×10^{-3}	0.181

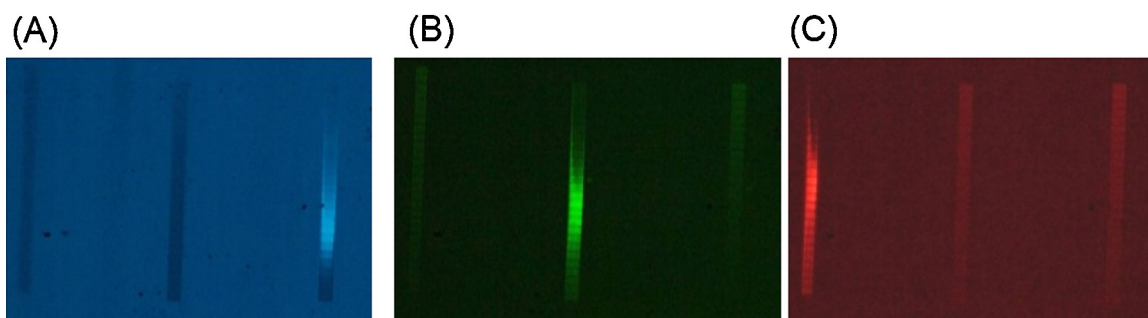


Fig. 4. Peak-tracking chip with 3 tracks of different periods targeting different resonant frequencies in the visible illuminated with monochromatic light of wavelengths (a) $\lambda = 480$ nm, (b) $\lambda = 550$ nm and (c) $\lambda = 630$ nm.

down and extract a small amount of oil (~ 10 mL). Extracted oil samples are filtered through 0.45μ pores syringe filter (Millipore™) to remove food suspended debris. In total, 40 cooking cycles were performed.

For animal fat and vegetable oil discrimination study, we use a mixture of pork fat and sunflower oil. Because animal fat is solid at room temperature, we perform such an experiment at a temperature of 40°C , by using backside resistance heaters on our chip holder, thus avoiding bulky incubator [14].

4. Results and discussion

4.1. Spectral properties in visible

Darkening of oil through successive cooking cycles is clearly observed by naked eye. Indeed, the colored degradation products formed by the interaction of food components with oil contribute to a color change. Suspended charred particles from the fried food induce a color change; this is however reduced through filtration. Other contributions are polymerization reactions at high temperatures. As a reference measurement, we characterize oil spectral properties through absorption spectroscopic measurements in visible. Fig. 5 gives the absorption spectra of oil samples extracted after a different number of cooking cycles.

A clear increase of absorption is observed at short wavelength (with even saturated absorption for 40 cooking cycles, through our 1 cm glass cell pathway). From the measurement, we also notice a small kink at short wavelength, in cooked oil spectra. To the best of our knowledge, this has not been reported elsewhere in details. It becomes more significant with the number of cooking cycles (or absorption), and might be due to a sharper absorption peak of some of the degraded oil components, or potato components. Refractive

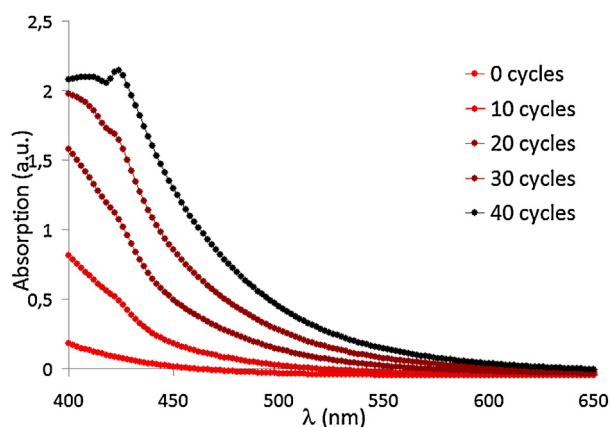


Fig. 5. Oil absorption spectra for different number of cooking cycles with arrow indicating tracks of our chip.

index also changes with an increasing number of cycles, with higher changes occurring where the absorption is higher, as predicted by Kramers Kronig relations [20].

Both the imaginary part (absorption) and the real part of the refractive index have effects on Fano resonance profiles. While a sole change in refractive index results in a shift of the resonant response (at least at first order), absorption affects the shape of the Fano response [8,21]. Based on spectral absorption measurements, we choose for this first demonstration wavelengths at which absorption can be neglected. Specifically, we perform measurements at a wavelength $\lambda = 630$ nm for cooked oil testing. Because animal fat gets solid at room temperature, spectroscopic absorption data could not be measured with our lab spectrometer. From observation by naked eye through a glass cell, warmed animal fat sample is transparent in the visible domain. Vegetable oil has low absorption (see Fig. 5, '0 cycle' sample) for $\lambda = 480$ nm and $\lambda = 630$ nm, and refractive index at both wavelengths were studied. Studying both real and imaginary part of refractive index is not trivial (contributions are intricate) [8,21] but extends the applications and the discrimination potential of the technique.

4.2. Oil quality sensing depending on the number of cooking cycles

The most characterized change of oil degradation is the increase content of total polar materials (TPM). Deep frying can increase TPM content ten times to over thirty percent, as revealed by column chromatography from many reports [22,23]. The polarizability that can be directly related to the refractive index through the Lorentz-Lorenz equation as follows:

$$(n^2 - 1)/(n^2 + 2) = (4\pi/3)\rho\alpha$$
 where α is molecular polarizability and ρ is the number density of polar molecules, so oil refractive index n will increase with the accumulation of polar material [5]. This gives us a convenient way for on-site detection of TPM increase during oil degradation.

The chip is first mounted on the fluidic holder, with an O-ring between the chip and fluidic holder pressed mechanically by outside screws to hold tight the fluidic chamber and for mechanical stability. Fluidic integration with black anodized aluminum holder and thermal controller using back-side resistance has been described in details [14]. We calibrate the chip with 3 reference solutions with refractive index covering the range of interest, and assume a good linearity on the small range. The calibrating solutions consist in glycerol-water mixture, with composition of 100:0, 99:1 and 98:2. At $T = 25^\circ\text{C}$ and $\lambda = 630$ nm, refractive index of glycerol and water are respectively of $n = 1.47075$ and $n = 1.3318$ for water. This corresponds to a difference in refractive index $\Delta n = 0.13895$. A change in 1% glycerol/water concentration corresponds to a change in refractive index of $\Delta n = 1.39 \times 10^{-3}$, and we

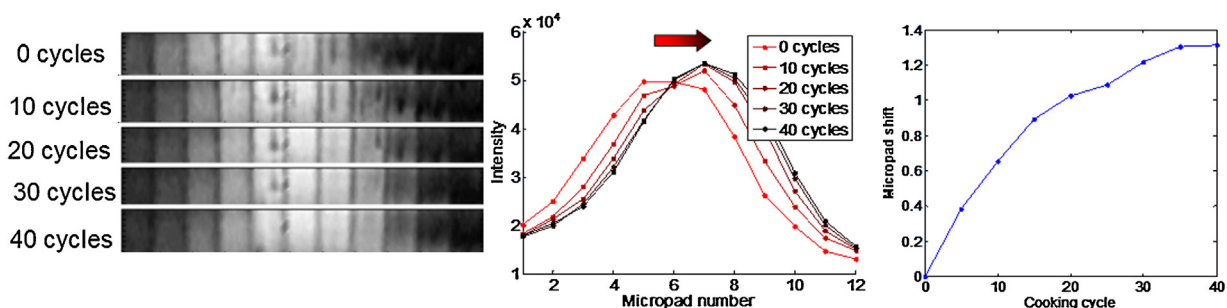


Fig. 6. (a) Track images at the wavelength of $\lambda = 630$ nm for different cooking cycles, (b) track profiles (c) peak shift determined by correlation analysis.

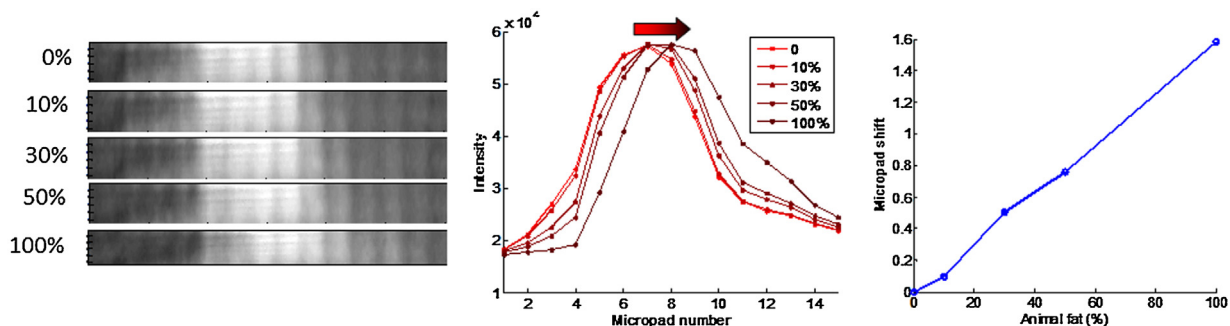


Fig. 7. (A) Track images at the wavelength for different composition of animal fat/sunflower oil at $\lambda = 630$ nm, (B) track profiles, (C) peak shift determined by correlation analysis.

have here a reference solution of refractive index of $n_{0\%} = 1.47075$, $n_{1\%} = 1.4694$, $n_{2\%} = 1.4680$. The experimental sensitivity of our chip is $PMS = 2 \times 10^{-3}$ RIU/micropad. Using our technique, we determine a refractive index of our sunflower oil solution to $n = 1.4693$, in agreement to other characterization [24].

We then determine the peak-shift of various oil samples (from 0 to 40 cooking cycles by step of 5 cycles). Measured pictures are given in Fig. 6(A) in gray scale color. A clear shift of the maximum intensity toward the right is observed. Fig. 6(B) shows line average profiles average of the micropads. For a good accuracy of peak position determination, we use correlation analysis to determine the peak shift whose robustness has been well assessed [13]. The peak shift is presented in Fig. 5(C) in micropad unit. From this figure, we clearly see a final peak shift of 1.35 micropad corresponding to a refractive index change from 1.4693 to 1.4720. The slope decreases as the number of cycle increases, with a $\sim 1.3 \times 10^{-4}$ /cycle at the beginning (~ 0.062 micropad/cycle), decreasing to $\sim 2.5 \times 10^{-5}$ /cycle from 20 cycles (~ 0.0165 micropad/cycle). From this graph, the observed change in refractive index at the wavelength of 630 nm is clear. This validates that our technique might be used for oil quality monitoring.

4.3. Oil discrimination depending on the composition in animal fat and vegetable oil

Another common property of “gutter oil” is their heterogeneous origin—mixture of animal fat and vegetable oil. To target this problem, we use a mixture of animal fat (from cooked pork) and sunflower oil. The content in animal fat is of 0%, 10%, 30%, 50% and 100%.

Since animal fat is solid at room temperature, spectroscopic measurement of liquid fat sample could not be performed with our spectrometer. Nevertheless, warmed at 40°C , animal fat is liquid and is seen transparent through a 1 cm glass cuvette. Fresh sunflower has also low absorption at $\lambda_b = 480$ nm (see Fig. 5). Therefore, at both wavelength $\lambda_b = 480$ nm and $\lambda_r = 630$ nm, the main expected contribution is a shift of the resonant profile.

Characterizations by ‘Peak-tracking chip’ imaging were performed at both $\lambda_r = 630$ nm and $\lambda_b = 480$ nm. Samples were pre-warmed at 40°C and a customized thermo-controlled chamber was used to maintain this temperature [14].

Similarly as in Fig. 6, we give in Fig. 7(A) the acquired pictures at $\lambda_r = 630$ nm, and in Fig. 7(B) the corresponding intensity profiles.

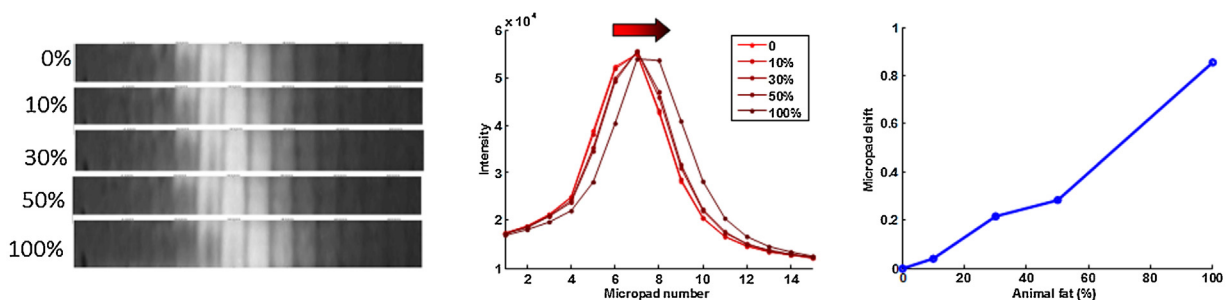


Fig. 8. (A) Track images at the wavelength for different composition of animal fat/sunflower oil at $\lambda = 480$ nm, (B) track profiles, (C) peak shift determined by correlation analysis.

We observe a shift of the resonant profile, whilst the change in diffraction efficiency and profile shape does not seem affected by absorption. The shift is determined using correlation analysis, and reported in Fig. 7(C). It is almost linear with the ratio of fat composition. Irregular data may come from the uncertainty of the sample preparation. Indeed, high viscosity of the samples as well as animal fat solid state at room temperature limited the accuracy in sample preparation.

At $\lambda_r = 630$ nm, the total measured shift is 1.6 micropad, corresponding to 3.2×10^{-3} change in refractive index considering a dispersion of 2×10^{-3} RIU/micropad from our chip calibration. This result is given in Fig. 7(C). We see here that a clear shift is measured by our technique, demonstrating that the change and sensitivity of our technique is good for such oil discrimination.

We then perform characterization at $\lambda_b = 480$ nm. Measured images are given in Fig. 8(A), while corresponding profiles are given in Fig. 8(B). The shift depending on the proportion of animal fat is reported in Fig. 8(C). The total shift is of 0.9 micropad. As seen previously the ratio in dispersion is estimated to $PMS_b/PMS_r = 2.2$. This corresponds to a change in refractive index of 4.0×10^{-3} at $\lambda_b = 480$ nm. From classical dispersion law of oil sample [25], a higher change in refractive index is expected at shorter wavelengths, and our experimental result is in agreement with this expectation.

5. Conclusions/outlook

Oil composition and oil degradation through cooking process result in a change of refractive index. Our present study demonstrated the measurement of oil refractive index variation through simple imaging of a nanostructured chip. Our technique sensitivity allows monitoring of oil quality, as demonstrated using sunflower oil with increasing number of cooking cycles. It can also be used to characterize various oils or oil mixture. Its flexibility in term of wavelength, tiny amount of sample cost and compact and usual instrumentation make it very suitable for on-site usage. It has high discrimination potential, as illustrated here with a mixture of 2 different oils, but which might be extended to a larger number of samples, for instance considering more wavelengths.

In recent years, miniaturization has brought many advantages in term of portability of devices, reduced consumption of biological samples and buffers for associated treatment, time and cost. Since their introduction, “smart” mobile phones encounter a large success, as witnessed by the number of users and the constantly increasing number of software applications. With their Internet connectivity, high-resolution cameras, touch-screen displays and powerful CPUs, it is very attractive to extend their possibilities to sensing. Recently, integrating biology applications in smartphone format has attracted much interest in science, with demonstrations in microscopy [26,27] as well as biodetection [28,29]. Our refractive index sensing chip can supply an ideal case for oil monitoring in a smart mobile phone format. One may take benefit of LED light source as well as camera CCD that are already part of the smartphone device. Specific holder might be made for the ‘peak-tracking chip’, with associated fluidic and optical elements, so that a drop of sample (for instance introduced with a pipette onto the chip and holder) can be analyzed.

Acknowledgments

We thank HKUST Nanofabrication facilities staff for their help in chip fabrication process and HKUST mechanical workshop for their help in the fluidic device fabrication. We thank Rachel A. McKendry and Tania Saxl for fruitful discussions. The electron beam lithography project is supported by University Grants Committee

reference SEG_HKUST10. The project is supported by RGC grant number 674710, as well as grant RPC11SC01.

References

- [1] D. Barboza, Recycled Cooking Oil Found to be Latest Hazard in China, New York Times (2010, March 31) <http://www.nytimes.com/2010/04/01/world/asia/01shanghai.html>
- [2] L.W. Clark, G.W. Serbia, Safety aspects of frying fats and oils, *Food Technol.* 45 (1991) 84–89.
- [3] Proposals Pouring in for Testing Gutter Oil, China Daily (2012, May 24) http://usa.chinadaily.com.cn/business/2012-05/24/content_15377554.htm
- [4] S. Paul, G.S. Mittal, Dynamics of fat/oil degradation during frying based on optical properties, *J. Food Eng.* 30 (1996) 389–403, [http://dx.doi.org/10.1016/S0260-8774\(96\)00020-9](http://dx.doi.org/10.1016/S0260-8774(96)00020-9)
- [5] H.A. Al-Kahtani, Survey of quality of used frying oils from restaurants, *J. Am. Oil Chem. Soc.* 68 (11) (1991) 857–862, <http://dx.doi.org/10.1007/BF02660602>
- [6] K. Bougot-Robin, S. Li, Y. Zhang, I.M. Hsing, H. Benisty, W. Wen, “Peak Tracking Chip” for label-free optical detection of bio-molecular interaction and bulk sensing, *Analyst* 137 (2012) 4785–4794, <http://dx.doi.org/10.1039/C2AN35994D>
- [7] K. Schmitt, K. Oehse, G. Sulz, C. Hoffmann, Evanescent field sensors based on tantalum pentoxide waveguides – a review, *Sensors* 8 (2008) 711–738, <http://dx.doi.org/10.3390/s8020711>
- [8] K. Bougot-Robin, J.L. Reverchon, M. Fromant, L. Mugheri, P. Plateau, H. Benisty, 2D label-free imaging of resonant grating biochips in ultraviolet, *Opt. Express* 8 (2010) 11472–11482, <http://dx.doi.org/10.1364/OE.18.011472>
- [9] E.M. Yeatman, Resolution and sensitivity in surface plasmon microscopy and sensing, *Biosens. Bioelectron.* 11 (6) (1996) 635–649, [http://dx.doi.org/10.1016/0956-5663\(96\)83298-2](http://dx.doi.org/10.1016/0956-5663(96)83298-2)
- [10] P. Li, B. Lin, J. Gerstenmaier, B.T. Cunningham, A new method for label-free imaging of biomolecular interactions, *Sens. Actuators B: Chem.* 99 (2004) 6–13, [http://dx.doi.org/10.1016/S0925-4005\(03\)00604-X](http://dx.doi.org/10.1016/S0925-4005(03)00604-X)
- [11] A.M. Ferrie, Q. Wu, Y. Fang, Resonant waveguide grating imager for live cell sensing, *Appl. Phys. Lett.* 97 (2010) 223704, <http://dx.doi.org/10.1063/1.3522894>
- [12] R.N. Clark, ‘Digital Camera Sensor Performance Summary’, 2012, Table 2, www.clarkvision.com/articles/digital_sensor_performance_summary
- [13] K. Bougot-Robin, W. Wen, H. Benisty, Resonant waveguide sensing made robust by on-chip peak tracking through image correlation, *Biomed. Opt. Express* 3 (2012) 2436–2451, <http://dx.doi.org/10.1364/BOE.3.002436>
- [14] K. Bougot-Robin, R. Kodzius, W. Yue, L. Chen, S. Li, X.X. Zhang, H. Benisty, W. Wen, Real time hybridization studies by resonant waveguide gratings using nanopattern imaging for Single Nucleotide Polymorphism detection, *Biomed. Microrev.* 16 (2014) 287–299, <http://dx.doi.org/10.1007/s10544-013-9832-2>
- [15] L. Li, Formulation and comparison of two recursive matrix algorithms for modeling layered diffraction gratings, *J. Opt. Soc. Am. A* 13 (1996) 1024–1035, <http://dx.doi.org/10.1364/JOSAA.13.001024>
- [16] A. David, High efficiency GaN-based LEDs: light extraction by photonic crystals, *Ann. Phys.* 31 (6) (2006).
- [17] L. Chen, M. Zhang, Z. Zhang, Dispersion compensation devices, in: Bishnu Pal (Ed.), *Frontiers in Guided Wave Optics and Optoelectronics*, 2010, <http://dx.doi.org/10.5772/39561>, ISBN: 978-953-7619-82-4, InTech.
- [18] R.L. Fork, O.E. Martinez, J.P. Gordon, Negative dispersion using pairs of prisms, *Opt. Lett.* 9 (1984) 150–152, <http://dx.doi.org/10.1364/OL.9.000150>
- [19] E.B. Treacy, Optical pulse compression with diffraction gratings, *IEEE J. Quantum Electron.* QE-5 (9) (1969) 454–458, <http://dx.doi.org/10.1364/JOSAB.3.000929>
- [20] R.de L. Kronig, On the theory of the dispersion of X-rays, *J. Opt. Soc. Am.* 12 (1926) 547–557, <http://dx.doi.org/10.1364/JOSA.12.000547>
- [21] U. Fano, Effects of configuration interaction on intensities and phase shifts, *Physiol. Rev.* 124 (1961) 1866–1878, <http://dx.doi.org/10.1103/PhysRev.124.1866>
- [22] Manral Mallika, M.C. Pandey, K. Jayathilakan, K. Radhakrishna, A.S. Bawa, Effect of fish (*Catla catla*) frying on the quality characteristics of sunflower oil, *Food Chem.* 106 (2008) 634–639, <http://dx.doi.org/10.1016/j.foodchem.2007.06.023>
- [23] S.M. Abdulkarim, H.M. Ghazali, Fatty acid ratios and their relative amounts as indicators of oil stability and extent of oil deterioration during frying, *Int. J. Food. Sci. Tech.* 10 (2012) 33–38.
- [24] Physikalisch Technische Bundesanstalt (PTB, Germany) *Physical Properties of Fats and Oils Ullmann's Encyclopedia of Industrial Chemistry*, vol. A 10, Fats and oils, VCH, Weinheim, 1995.
- [25] A. Soraya, Khodier, Refractive index of standard oils as a function of wavelength and temperature, *Opt. Laser Technol.* 34 (2002) 125–128, [http://dx.doi.org/10.1016/S0030-3992\(01\)00101-3](http://dx.doi.org/10.1016/S0030-3992(01)00101-3)
- [26] Q. Wei, H. Qi, W. Luo, D. Tseng, S.J. Ki, Z. Wan, Z. Göröcs, L.A. Bentolila, T.T. Wu, Fluorescent imaging of single nanoparticles and viruses on a smart phone, *ACS Nano* 7 (2013) 9147–9155, <http://dx.doi.org/10.1021/nn4037706>
- [27] I. Navruz, A.F. Coskun, J. Wong, S. Mohammad, D. Tseng, R. Nagi, S. Phillips, A. Ozcan, Smart-phone based computational microscopy using multi-frame contact imaging on a fiber-optic array, *Lab Chip* 13 (2013) 4015–4023, <http://dx.doi.org/10.1039/c3lc50589h>
- [28] A.F. Coskun, R. Nagi, K. Sadeghi, S. Phillips, A. Ozcan, Albumin testing in urine using a smart-phone, *Lab Chip* 13 (2013) 4231–4238, <http://dx.doi.org/10.1039/c3lc50785h>

- [29] D. Gallegos, K.D. Long, H. Yu, P.P. Clark, Y. Lin, S. George, P. Nath, B.T. Cunningham, Label-free biodetection using a smartphone, *Lab Chip* 13 (2013) 2124–2132, <http://dx.doi.org/10.1039/c3lc40991k>.

Biographies

K. Bougot-Robin received an engineering degree from ESPCI in Paris, with a specialization in Bio-engineering (2006). She graduated from a PhD in biophotonics of Paris XI University (2009), in collaboration with Thales Research and Technology. She pursued as postdoctoral Fellow in Institute of Advanced Study in Hong Kong University of Science and Technology HKUST (2010–2013). She is now research associate at Imperial College London. Her research interest include Optics, Nano/microfabrication, Characterization, Materials, Sensors, Biology/health applications, Fluidic, Modeling, Nanopores.

W. Cao is currently a PhD student at the Hong Kong University of Science and Technology with a research focus on microfluidic biosensor and mechanic properties of cell. He received his BSc (2002) in plant protection at the Huazhong Agricultural University in Wuhan. He completed his MPhil (2005) thesis in carbon nano materials at the Institute of High Energy Physics, CAS, Beijing.

S. Li received his BS degree in Physics from Chongqing University, Chongqing, China, in 2009. Then he joined the Hong Kong University of Science and Technology, Hong

Kong, China, where he obtained his PhD degree. After that he moved to School of Chemistry at University of Leeds, where he is currently a postdoc research fellow. His research interest is mainly focused on Micro/Nanofluidics, Micro/Nano-fabrication for Microdevices and functional electromagnetic materials, and Biomineralization.

H. Benisty received the PhD degree from University Paris 6, Paris, France in 1989. Since 1994, he has been involved in research on microcavities and in photonic crystals in two dimensions on III-V semiconductors in laboratory PMC, Palaiseau, France. He was with University of Versailles until 2002 and is since 2002 with Institut d'Optique in Palaiseau, laboratoire Charles Fabry. He investigates applications of periodic nanostructures to LEDs, biophotonics, various blocks of miniature photonic integrated circuits and multimode structures, and novel plasmonic hybrid waveguides. He co-founded a biochip-related company Genewave, recently merged with MobidiagOy (Helsinki).

W. Wen earned his BS (1982) and MS (1988) degrees at Chongqing University. He completed his PhD (1995) degree in Institute of Physics, Chinese Academy of Science, Beijing. He was a postdoctoral fellow at HKUST (1995–1997) and UCLA (California University at Los Angeles) (1997–1999). He joined HKUST in 1999 and currently is a professor in the department of Physics, HKUST. Professor Wen's main research interests include soft condensed matter physics, electrorheological (ER) and magnetorheological (MR) fluids, field-induced pattern and structure transitions, micro- and nano-fluidic controlling, microsphere and nanoparticle fabrications, thin film physics, metamaterials and nonlinear optical materials